Comparison of spatial downscaling methods of general circulation models to study climate variability during the Last Glacial Maximum

Guillaume Latombe[1,2], Ariane Burke[3], Mathieu Vrac[4], Guillaume Levavasseur[5], Christophe Dumas[4], Masa Kageyama[4], Gilles Ramstein[4]

[1]Department of Mathematical Sciences, Stellenbosch University, Matieland 7602, South Africa
[2]School of Biological Sciences, Monash University, Melbourne 3800, Australia
[3]Département d'anthropologie, Université de Montréal, Montréal, QC, Canada
[4]Laboratoire des Sciences du Climat et de l'Environnement/Institut Pierre-Simon Laplace, Université Paris-Saclay, CE Saclay, l'Orme des Merisiers, Bât.701, Gif-sur-Yvette, France
[5]Institut Pierre Simon Laplace (IPSL), Pôle de modélisation du climat, UPMC, Paris, France

Correspondence to: Guillaume Latombe (latombe.guillaume@gmail.com)

Abstract. The extent to which climate conditions influenced the spatial distribution of hominin populations in the past is highly debated. General Circulation Models (GCMs) and archaeological data have been used to address this issue. Most GCMs are not currently capable of simulating past surface climate conditions with sufficiently detailed spatial resolution to distinguish areas of potential hominin habitat, however. In this paper we propose a Statistical Downscaling Methods (SDM) for increasing the resolution of climate model outputs in a computationally efficient way. Our method uses a generalized additive model (GAM), calibrated over present-day data, to statistically downscale temperature and precipitation from the outputs of a GCM simulating the climate of the Last Glacial Maximum (19-23,000 BP) over Western Europe. Once the SDM is calibrated, we first interpolate the coarse-scale GCM outputs to the final resolution and then use the GAM to compute surface air temperature and precipitation levels using these interpolated GCM outputs and fine resolution geographical variables such as topography and distance from an ocean. The GAM acts as a transfer function, capturing non-linear relationships between variables at different spatial scales. We tested three different techniques for the first interpolation of GCM output: bilinear, bicubic, and kriging. The results were evaluated by comparing downscaled temperature and precipitation at local sites with paleoclimate reconstructions based on paleoclimate archives (archaeozoological and palynological data). Our results show that the simulated, downscaled temperature and precipitation values are in good agreement with paleoclimate reconstructions at local sites confirming that our method for producing fine-grained paleoclimate simulations suitable for conducting paleo-anthropological research is sound. In addition, the bilinear and bicubic interpolation techniques were shown to distort either the temporal variability or the values of the response variables, while the kriging method offers the best compromise. Since climate variability is an aspect of their environment to which human populations may have responded in the past this is an important distinction.

1 Introduction

The extent to which past climate change influenced human population dynamics during the course of prehistory is a subject of lively debate. The Last Glacial period, including Marine Isotope Stages 3 (MIS3) and 2 (MIS2) and the Last Glacial Maximum (LGM), is particularly interesting in the context of this debate (van Andel, 2003). During MIS3 the archaeological

5   record suggests that modern human populations originating in Africa expanded into Eurasia, while Neanderthal populations progressively contracted their range before becoming extinct ~27,000 years Before Present (BP) (Serangeli and Bolus, 2008). Progressively colder and drier conditions, culminating in the LGM (19,000 - 23,000 years Before Present), are thought to have triggered further range contractions and the demographic decline of modern human populations in Europe. Climate affects the spatial behaviour of human populations directly (when conditions exceed human physiological limits)

10   and indirectly (when it affects the distribution of resources upon which humans depend).The global climate during the Last Glacial period was characterised by a series of rapid oscillations (known as Dansgaard-Oeschger, or D-O events). These events may have acted as forcing mechanisms, affecting the demographic processes described above (e.g. Müller et al., 2011; Schmidt et al., 2012; Sepulchre et al., 2007; Jimenez-Espejo et al., 2007; Banks et al., 2013; d'Errico and Sánchez Goñi, 2003; Gamble et al., 2004; Shea, 2008). While the timing of climate events relative to large-scale patterns in the

15   archaeological record is suggestive, the mechanisms by which climate forcing acted on human populations are still imperfectly understood. More empirical evidence is needed to validate the hypothesis that climate forcing affected human population dynamics and explore the nature and scale of the effect.

The broad demographic patterns mentioned above are the result of smaller, local-scale patterns produced by mobile groups

20   of hunter-gatherers distributing themselves on the landscape in order to exploit available resources. The availability of these resources fluctuated both predictably (on a seasonal basis) and unpredictably (as a result of climate variability). It is by gaining an understanding of these smaller-scale patterns, ultimately, that we will be able to understand how climate forcing affects the spatial and cultural dynamics of prehistoric human populations. Previous analyses of climate forcing have used a variety of data to reconstruct the paleoclimate, such as ice-core or marine records (e.g., Bradtmöller et al., 2012; Jimenez-

25   Espejo et al., 2007; Schmidt et al., 2012), present-day climate data (e.g., Jennings et al., 2011), and climate model simulations (e.g., Banks et al., 2008; Davies and Gollop, 2003; Sepulchre et al., 2007; Benito et al. 2017; Hughes et al. 2007; Tallavaara et al. 2015). These analyses were conducted at varying spatial resolutions, typically on the order of ~50 km x 50 km (= 2500 km^2). The goal of this study is to develop high-resolution climate simulations suitable for the quantification of climate variability at an inter-annual scale and a spatial scale of ~15 km x 15 km (= 225 km^2) which approximates the size of

30   the catchments within which hunter-gatherer groups forage (Vita-Finzi and Higgs, 1970) making this an ideal spatial scale at which to consider the impact of climate variability on human systems.

Global Climate Models (GCMs) are able to simulate climate conditions at various spatial and temporal scales, whereas

climate proxy data are inherently limited by the uneven distribution of sample locations and taphonomic biases (pollen preservation, location of archaeological sites, etc.). GCMs use physical equations, e.g. to represent atmospheric fluid dynamics, as well as parameterisations, e.g. for sub-grid scale phenomena, to simulate the Earth's climate. The major disadvantage of GCMs is that they are computationally intensive and are usually only used to model climate behaviour at

5   relatively coarse spatial resolution, typically coarser than 100 km (cf. Flato et al., 2013 for the latest details on the CMIP5 models) especially for long paleoclimatic simulations. Their ability to simulate the small-scale physical processes that drive local surface variables, such as precipitation, is therefore limited (Wood et al., 2004).

Regional Climate Models (RCM) represent a physically based approach to climate modelling at a finer spatial scale over a

10   specific region of interest (*e.g.*, Liang et al., 2006, Flato et al., 2013). However, RCMs use GCM outputs to set their boundary conditions. They therefore require the explicit modelling of the physical processes at both coarse and fine scales over the whole planet and over region of interest, respectively, and are also computationally demanding. Statistical Downscaling Methods (SDM), on the other hand, are less computationally demanding. SDMs proceed by empirically associating local-scale variables with large-scale atmospheric variables produced by GCMs, and are faster to compute than

15   mechanistic RCMs (Vaittinada Ayar et al., 2015). SDMs fall into four main families: "transfer functions", which directly link large-scale and local-scale variables; "weather typing" methods based on conditioning statistical models on recurrent weather states; "stochastic weather generators" that simulate downscaled values from their (potentially conditional) probability density functions; and "Model Output Statistics" (MOS) methods based on adjusting (i.e., correcting) the statistical distribution of the large-scale GCM simulations in order to generate local-scale variables with the correct statistical

20   properties (e.g., Vaittinada Ayar et al., 2015).

In this study, we apply an SDM from the transfer functions family, based on Generalized Additive Modelling (GAM), to compute temperature and precipitation at a fine spatial resolution for the LGM over Western Europe. We use a 50 year-long time series of climate simulations for the LGM (Kageyama et al., 2013a, b) and the present climate (Dufresne et al., 2013)

25   extracted from the IPSL-CM5A-LR GCM (Dufresne et al., 2013). GAM is a non-parametric statistical technique that has proven reliable for capturing non-linear relationships between local- and large-scale variables (e.g., Vrac et al., 2007; Levavasseur et al., 2010). In the present study, interpolated values of coarse-grain variables extracted from the GCM, as well as fine-scale geographical data such as elevation and advective continentality, are used as predictors in the GAM. The result is the production of downscaled monthly values for temperature and precipitation. We compare the impact of three different

30   interpolation techniques (bilinear interpolation, bicubic interpolation and kriging) on the downscaling, evaluating the resulting SDM outputs with the aid of climate proxies (palynological and archaeozoological data) and observing the impact of each technique on the calculation of temporal variability in temperature and precipitation.

2 Materials and Methods

2.1 Global Climate Model

The GCM used in this study is the ocean-atmosphere coupled model IPSL-CM5A-LR (Dufresne et al., 2013) developed for the CMIP5 (Taylor et al., 2012) and PMIP3 (Braconnot et al., 2012) projects and the 5th IPCC report (IPCC, 2013). The

5 IPSL-CM5A-LR model has a spatial resolution of 1.9° in latitude and 3.75° in longitude over Europe, which is the area of interest here (i.e. ~62 500 km^2).

A present-day simulation was run according to the CMIP5 protocol, for the period from 1960 to 1990 with the corresponding forcings in atmospheric composition and land use changes. Outputs from this simulation are used in the calibration process

10 (below). The simulation of LGM climate conditions follows the PMIP3 protocol (Braconnot et al., 2011, Braconnot et al., 2012). The concentrations of atmospheric greenhouse gases were lowered to their LGM values derived from ice core data (185 ppm for CO_2, 350 ppb for CH_4 and 200 ppb for N_2O) and the ice sheets are prescribed according to the product developed for PMIP3 (Abe-Ouchi et al., 2015). The model is run for several hundred years until the response to the LGM forcing in terms of surface climate variables is stabilised (Kageyama et al., 2013a, b). For this research, we extracted 50

15 years of monthly mean data (temperature 2m above the surface, precipitation, sea level pressure and relative humidity) from the stabilised part of the simulation. Next, we downscaled the data, calculated their average climatology and their temporal (interannual) variability.

2.2 Generalized additive models

Generalized additive models (GAM, Hastie and Tibshirani, 1990) are statistical models blending the properties of

20 generalized linear models with additive models. Given a dependent variable Y and p predictor variables $[X_1,…,X_p]$, GAMs compute $E(Y| X_1,…,X_p)$, the expected value of Y, conditionally on the p predictors X_i, as a sum of non-parametric functions as follows:

$$E(Y|X_1,…,X_p) = \sum_{i=1}^{p} f_i(X_i),$$
(1)

Following Vrac et al. (2007), cubic spline functions were used for the f_i, represented by piece-wise third-order polynomial functions. For each function f_i, a number of knots are placed evenly throughout the predictor range, and the cubic polynomials that compose f_i are constrained to continuity conditions at each knot to ensure smooth transitions (Wood, 2000, 2004). GAMs were calibrated using the mgcv package (Wood, 2006) in R, and the number of knots was determined

30 automatically using generalised cross-validation.

Using a combination of geographical and physical predictor variables has been shown to improve spatial downscaling results

(Vrac et al., 2007). Using GAMs on climate variables requires the predictor and dependent variables to have the same spatial scale. The present-day dependent variables (precipitation and temperature) are at a fine spatial scale. The elevation variable is also at a fine spatial scale, whereas the predictor climate variables generated by the GCM are at a coarser scale. Thus, interpolation of the predictor climate variables is necessary.

Once the functions f_i have been fitted using the present-day data, the downscaling can be performed on the GCM outputs for the LGM. The downscaling uses fine-scale and interpolated predictor climate variables corresponding to the LGM to generate fine-scale dependent variables. Here, two GAMs are calibrated: one for temperature and one for precipitation.

2.3 Calibration data

2.3.1 Fine-scale dependent variables: the CRU climatology.

Fine-scale, present-day temperature and precipitation dependent data were obtained from the Climate Research Unit (CRU, New et al., 2000). The spatial resolution of the data is 10' (*i.e.* 1/6 degree), regularly gridded between 32.72° and 59.861° latitude (N = 164 values) and -11.578° and 24.738° longitude (N = 219 values) for a total of N = 35916 grid-points. We computed a monthly climatology for each gridpoint by averaging the variable of interest (temperature or precipitation) over 31 years (from 1960 to 1990) for each month (Fig. S1).

2.3.2 Large-scale predictor variables.

We used the data from a CMIP5 historical simulation run with the IPSL-CM5A-LR model to produce the predictor climate variables used for the calibration of the GAMs. We calculated monthly climatological averages from the simulation outputs for the period from 1960 to 1990, i.e. the same years as for the CRU data (see above). The predictor variables we used are: temperature (T), precipitation (P), atmospheric pressure at sea level (SLP) and relative humidity (RH). The variables were spatially interpolated to match the spatial resolution of CRU data, which is 10'; each grid-point in the CRU data therefore matches a value for each of the predictor variables. Three interpolation methods were tested: bilinear, bicubic and kriging (Figs. S2-S4). For the kriging method, we used the "krig" function from the vacumm python package (http://relay.actimar.fr/~raynaud/vacumm/) using an exponential fit of the variogram, with the fit computed independently for every month and every variable interpolated variable.

2.3.3 Fine-scale predictor variables.

We extracted present-day elevation data from the CRU dataset gridded at the same fine-scale spatial resolution as the dependent variables. We computed the advective (Aco) and diffusive (Dco) continentalities, following Vrac et al. (2007). Dco is bounded between 0 and 1, and corresponds to the shortest distance to the ocean. A low value means that distance to the ocean is small, and *vice versa*. Aco is also bounded between 0 and 1, and takes the direction and intensity of prevailing

winds into account along with the distance to the ocean. Both variables are used to account for the fact that an air mass becomes more continental as it travels across land. Since Dco and the Aco proved to be highly correlated but Aco provided the best performance in the models, we only selected Aco for the present analysis (Figs. S2-S4).

2.4 Calibration of the GAMs

5   For each dependent variable (temperature and precipitation) and for each interpolation technique (bilinear, bicubic and kriging), we tested different combinations of physical and geographical predictor variables. To downscale temperature, we computed GAMs for all possible combinations of coarse-grain temperature values from the GCM interpolated at fine scale, with fine-grain elevation and advective continentality (Aco), resulting in seven possible models for each interpolation. To downscale precipitation, we computed GAMs for all possible combinations of coarse-grain temperature, coarse-grain

10 precipitation, sea-level pressure, and relative humidity values from the GCM interpolated at fine scale, with fine-grain elevation and advective continentality (Aco), resulting in 31 possible models for each interpolation. For each interpolation technique, the resulting GAMs were compared using the Akaike Information Criterion (AIC; Akaike, 1974), and the model with the lowest AIC was selected. The AIC is a measure of the relative goodness of fit of each of the models and penalizes the number of parameters, thus preventing overfitting. The significance of each variable was assessed using p-values, and

15 verified by visual inspection of the spline 95% confidence intervals. Six GAMs were therefore retained after calibration (one for each response variable and for each interpolation technique)

2.5 Downscaling of temperature and precipitation for the LGM

We computed downscaled temperature and precipitation values using the six GAMs resulting from the calibration process described above, i.e. for the same predictor variables. The large-scale climate variables were generated by the GCM using

20 the PMIP3 protocol for the LGM prior to interpolation (Figs. S5-S7). The geographical variables are derived from a digital elevation model for the LGM (Levavasseur et al., 2011). In particular, the change in coastlines due to the lower sea-level at LGM is accounted for, which has an impact on the continentalities. The downscaling was performed for each month of the 50-year-long monthly output from the GCM, in order to obtain a long time series of fine-scale temperature and precipitation values over Europe and calculate climatological averages as well as variability and extremes.

25 ### 2.6 Evaluation data (palynological data and vertebrate remains)

To evaluate the performance of the SDM, we compared our temperature and precipitation outputs to local climate variables estimated on the basis of pollen and vertebrate fossils from 29 test locations (Table S1, Fig. S8). For each of our 29 test sites, we estimated the mean, minimum, and maximum temperature and precipitation rate on a monthly basis over the course of the 50 downscaled, simulated years, and compared the ranges of downscaled, simulated values to the ranges of values

30 reconstructed using the palynological data and vertebrate remains.

Reconstruction of local temperature and precipitation values were obtained from pollen data reported in an independent study using inverse vegetation modelling for 10 sites located in the Iberian peninsula (Wu et al., 2007). For the remaining 19 sites, vertebrate remains from another study (Burke et al. 2014) were used to calculate bio-climate indices (ff. Hernandez Fernandez, 2001a, b). The method set forth by Hernandez-Fernandez uses large and small vertebrates to compute the relative

5 probability that a given assemblage reflects one of Walter's nine global zonobiomes (Walter and Box, 1976). The method is based on the "climate envelope" method commonly employed in biogeographical reconstructions. The BCI uses presence/absence data, thus avoiding the problems inherent with calculating the relative representation of species from the archaeozoological record, and all available taxa rather than one or two "indicator" species, thus avoiding the risk that changes in the distribution of a single taxon could bias the biogeographical reconstruction. Ranges of temperature and

10 precipitation values for each zonobiome were estimated by mapping the modern distribution of zonobiomes in the northern hemisphere and compiling present-day temperature and precipitation data from the CRU data (see Burke et al. 2014). The zonobiomes (calculated using BCI) were then used to predict the climate ranges for each test location. Because archaeozoological assemblages are thanatocoenoses, rather than biocoenoses, they may represent more than one biome. Thus, we considered the two most probable zonobiomes (the two highest BCIs) for each site.

15 **2.7 Variability indices**

We calculated indices of variability, including measures of variance and inter-annual variability for the variables of interest. The standard deviation of monthly mean temperatures for each month was calculated for the 50-year run. The coefficient of variation of monthly mean precipitation values was calculated for the same period. Next, we used the Standardized Precipitation Index (Agnew 2000; Guttman 1999; McKee et al. 1993) to calculate how often a given month deviated from

20 expected precipitation values based on the climatic norm (calculated over 50 years) using a subroutine of the "SPEI" package in R (Vicente-Serrano et al. 2010) and a 12-month interval to standardize the values. Standardized Precipitation Index (SPI) values were then classified as "normal", "very" dry/wet, "severe" dry/wet and "extreme" dry/wet following McKee et al. (1993) and the number of "normal" months was summed to produce the variability index for Precipitation. The Standardized Temperature Index (STI), which is based on the same principle as the SPI, was calculated using the "STI"

25 package in R (Fasel 2014) and used to produce a variability index for temperature.

3. Results

3.1 The GAM

The best models (i.e., the models with the lowest AIC value) for temperature and for precipitation were obtained by using the same sets of variables (one for temperature, one for precipitation) in the GAM for the three interpolation techniques. The

30 predictors for temperature are: simulated temperature from the GCM, elevation and advective continentality (explaining 95.80%, 95.29% and 95.63% of the variance for the bilinear, bicubic, and kriging interpolations, respectively). For

precipitation, the predictors are: simulated temperature, precipitation, sea-level pressure and relative humidity from the GCM, elevation, and advective continentality (explaining 64.65%, 64.79% and 65.43% of the variance for the bilinear, bicubic, and kriging interpolations) (Table 1). The p-values for all variables for all models were < 0.001.

5   The splines resulting from the calibration process for the downscaling of temperature values show that fine-scale temperature readings are related to the GCM temperature and to elevation in a linear fashion, and the differences between the three interpolation techniques tested are negligible (Fig. 1). The fine-scale temperature is proportional to the GCM temperature but it is inversely proportional to elevation, which means that the GCM overestimates temperatures for high elevations. This is expected because temperature generally decreases with increasing altitude and because in the coarse grain GCM, it is the

10   average elevation over the grid box that is considered. Although the model including all three predictor variables produced the lowest AIC, advective continentality has a very limited impact on temperature, as the values of $f(\text{Aco})$ remain close to 0. When applied outside the range of values for which they were calibrated, GAMs use a linear extrapolation of the splines. The range of values for elevation is similar for the present-day and the LGM periods (Fig. 2). Because of the increased land mass during the LGM (which correlates with a low sea-stand), there are more high values for advective continentality, but

15   this difference should have a small impact since the spline is relatively flat for this variable. As expected, temperature is lower during the LGM than for present-day. This should nonetheless have a limited impact on projections because the linear interpolation of the spline outside of the range of values used for calibration is consistent with the fact that the spline is relatively linear for temperature.

20   The splines for the downscaling of precipitation, in contrast, are non-linear (Fig. 3). The splines showing the influence of temperature on expected precipitation rates show larger variations due to a low expected precipitation for both low and high temperatures, but high expected precipitation for middle-range temperatures. Although the expected precipitation increases monotonically with the interpolated precipitation rates, the spline values are lower than the GCM precipitation values and the relationship is non-linear. The expected precipitation increases more rapidly for low than for high interpolated precipitation,

25   in keeping with previous observations that GCMs (and even RCMs) overestimate drizzles, which may explain this correction (e.g. Gutowski et al.,2013). The three interpolation techniques produced similar splines for all variables, although the splines of the bicubic interpolation are slightly distinct from the other two interpolation techniques. The main difference is observed for the spline of the bicubic relative humidity, which indicates lower precipitation for low relative humidity than the other two interpolation techniques. Advective continentality is the variable with the least impact on precipitation rates. The ranges

30   of values for simulated precipitation, relative humidity, and for elevation are similar for the present-day and the LGM periods, and the distributions of the variable substantially overlap, indicating that the splines calibrated over the present-day period can apply for the LGM (Fig. 2). As for temperature, the spline of advective continentality is relatively flat, and the difference of range of values will have limited impact on the projections. Similarly, the simulated atmospheric pressure at sea level was lower for the LGM than for the present-day period, but the corresponding spline calibrated on present-day data

is linear at low values, and has little influence on the projections. For temperature, the splines are relatively linear near the lower end of the range of present-day values, and the linear interpolation of the spline at lower values for the LGM is therefore sensible.

3.2 Projections for the LGM

3.2.1 Temperature

Downscaled annual mean temperature was very similar for the three interpolation techniques tested (Figs. 4, 5). This was expected, since the splines for the GCM temperature and elevation for all three techniques are also very similar. Temperatures interpolated with the bilinear and kriging techniques were more similar to each other than to the temperature interpolated using the bicubic technique before (Figs. S9, S10) and after (Fig. 5) applying the GAMs. The differences between the bilinear and kriging techniques were regularly spaced, corresponding to the original coarse-grain cells from the GCM. This illustrates the difference between the two interpolation techniques: kriging generates smoother variations than the bilinear interpolation, which generates discontinuous variations at the original points. This difference remained after applying the GAMs, showing the impact of the interpolation technique used on the final outcome of the downscaling.

The main differences between the interpolated and downscaled temperatures occur in the North-East region of Europe (Fig. S11), with the downscaled temperature being higher, especially in winter. This difference was also observed when comparing present-day CRU data with the interpolated GCM data (Fig. S12), although with a much lower amplitude. North-East Europe is the coldest region of the study area for both the LGM and the present-day (Figs. S2-S7). Since the spline for temperature has a slope lower than 1 for low temperatures (Fig. 1), the GAM generates higher temperatures than the interpolated values, especially for very low temperatures falling outside of the present-day range of values due to the linear interpolation of the spline. As a result, the difference between the interpolated and downscaled temperature during the LGM is lower in summer. The SDM also took fine scale variations in topography into account, such as abrupt elevation changes in the Alps and Pyrenees (Fig. S11).

The range of temperatures for the 19 sites for which the BCIs were computed are in accordance with the temperature reconstructions, irrespective of the interpolation technique used (Fig. 6). Simulated temperature ranges fall within the reconstructed ranges corresponding to the primary BCIs for all sites (Fig. 6a,c,e). The reconstructions from Wu et al. (2007) produce smaller ranges of values, but the simulated ranges overlap with reconstructed temperatures (Fig. 6b,d,f).

3.2.2 Precipitation

Bilinear interpolation and kriging resulted in very similar downscaled precipitation values, whereas the precipitation rates predicted using bicubic interpolation were substantially lower in the South-West of Europe in winter and higher in the North

of Europe (over the current North Sea) in Summer (Figs. 7, 8). This result is consistent with the observation that the splines for the bicubic interpolation differed from the other two techniques. The three interpolation techniques produced similar distributions of precipitation rates, but compared to the two other interpolation techniques the results of the bicubic interpolation differed the most (Figs. S13, S14). A comparison of interpolated and downscaled precipitation for the LGM

5   with all three interpolation techniques shows that the GCM underestimates precipitation over the South of Europe and overestimates it over the North in winter, and substantially underestimate precipitation over all of Europe in Summer (Fig. S15). Comparing GCM projections interpolated at fine scale with the present-day CRU data confirms this pattern in winter, and shows that the GCM overestimates precipitation over the South of Europe and underestimates them over the North in Summer (Fig. S16), which results in the non-linear spline for precipitation (Fig. 3). This is due to the fact that GCMs

10   perform poorly when simulating the small-scale physical processes that drive local surface variables such as precipitation (Wood et al., 2004).

Precipitation ranges for the 19 sites for which the BCIs were computed are in accordance with the precipitation ranges reconstructed for the LGM. Simulated precipitation ranges for all sites fall within the reconstructed ranges corresponding to

15   the primary and secondary BCIs (Fig. 9). As with temperature, the reconstructions from Wu et al. (2007) show smaller ranges of precipitation than the reconstructions using the BCIs.

3.2.3 Variability

The temporal variability of temperature and precipitation showed important differences between the three interpolation techniques. When temporal variation was computed over the interpolated variables (Figs. S17, S18), bilinear interpolation

20   showed regular spatial patterns for both temperature and precipitation, especially in summer. This pattern was less apparent for kriging, and almost absent for bicubic interpolation.

With bilinear interpolation, the interpolated values will necessarily have a lower variation (whatever the index used) than the original values. For a simple linear interpolation, given 2 spatially consecutive values at 2 different points in time ($y(x_0,t_0)$,

25   $y(x_0,t_1)$, $y(x_1,t_0)$ and $y(x_1,t_1)$), any linearly interpolated value $y(x_i)$ for a location x_i in $[x_0, x_1]$ will necessarily be comprised in $[y(x_0),y(x_1)]$. In addition, due to the linear interpolation $|y(x_i,t_1)- y(x_i,t_0)| < |y(x_0,t_1)- y(x_0,t_0)|$ and $|y(x_i,t_1)- y(x_i,t_0)| < |y(x_1,t_1)-y(x_1,t_0)|$. By contrast, since kriging does not impose linear interpolation between x_0 and x_1, this relation does not necessarily hold, and even less for bicubic interpolation, which do not impose $y(x_0) \leq y(x_1) \leq y(x_1)$. However, because of this absence of restriction, bicubic interpolation can generate values with a high variability, as for precipitation in summer in the South-West

30   of the Iberian peninsula (Fig. S18; the high variability for kriging in winter only occurs at the boundary of the study area due to boundary conditions, and can therefore be discarded).

Computing temporal variation over the downscaled variables (Figs. 10, 11), showed that the GAMs attenuated this spatial patterns, which nonetheless still occurred for the bilinear interpolation, and was almost non-existent for the other two interpolation techniques.

5   The three interpolation techniques generated similar STI and SPI surfaces (Fig. S19). The main difference occurred for the SPI from the bicubic interpolation, which showed less months with "normal" precipitation (i.e. either drier or wetter than baseline) than the other two interpolation techniques in the center and North of Europe. As for the temporal variability, this result is due to the fact that, contrary to the other two interpolation techniques, bicubic interpolation generates values outside of the original coarse-scale values, and is therefore more likely to over- or underestimate them.

10   **4 Conclusion and Discussion**

We apply GAM-based statistical downscaling, a computationally efficient method for the downscaling of large-scale climatic variables from global climatic models (Vrac et al. 2007), to the downscaling of temperature and precipitation values produced by the IPSL-CM5 model for 50 simulated years over Western Europe during the last glacial maximum. A single GAM was used for each dependent variable, calibrated over the average of 31 years present-day data. Comparing the outputs
15   of the SDM with two different climate reconstructions showed that the method produced satisfying results. It also enabled us to compute indices of climate variability. Elsewhere, we demonstrate that climate variability is a key factor governing the spatial distribution of human populations society during the LGM (Burke et al. 2014, 2017). Nonetheless, SDMs require a careful evaluation of the different variables considered.

20   The interpolation technique used in the SDM proved critical for the accuracy of the output. Since the GAMs require the predictor and the dependent variables to have the same spatial grain, bilinear interpolation is commonly used to downscale the coarse-grain data generated by the GCM (Vrac 2007). However, bilinear interpolation is shown to generate non-smooth surfaces, which may cause spatial artifacts in the final output. We tested two other non-linear interpolation techniques which generate smoother surfaces: bicubic interpolation and kriging. Bicubic interpolation generates values outside of the initial
25   range of values (and therefore under- or overestimates the values) but is faster to apply than Kriging. Kriging is more computationally demanding but offers the advantage of constraining the interpolated values within the range of initial values. The three interpolation techniques showed differences for both temperature and precipitation during the LGM (Figs. S10, S14). After applying the GAM, these differences were especially important for precipitation values (Fig. 8). In particular, bicubic interpolation predicts drier environments than the other two techniques by up to 2 mm/day. Since GCMs operate at
30   grains that are too coarse to accurately model small-scale physical processes driving local surface variables (Wood et al., 2004), the SDM for precipitation relies on more variables than the temperature. The splines for these variables are non-linear, which may explain the important differences between the SDM based on bicubic interpolation and the SDM based on

the other two techniques. The cumulative impact of the interpolation and the GAM can therefore be non-negligible. This pinpoints the utility of the comparison presented here, especially for local phenomena such as precipitation.

Moreover, the variability maps produced when using bilinear interpolation show the presence of a spatial artefact, in the
5   form of a regular grid, for both temperature and precipitation (Figs. S17, S18). This artefact reflects the fact that bilinear interpolation generates lower variability between the points from which the interpolation is performed. Although slightly attenuated, this artefact remained after applying the GAMs (Figs. 10, 11). Prior to applying the GAMs, bicubic interpolation produced maps with the smallest level of artifacts and kriging was intermediate. However, bicubic interpolation sometimes generated unrealistically high variability for precipitation (Fig. S18). After applying the GAMs, the artifact generated by
10   kriging decreased (Figs. 10, 11).

Assuming that the range of values of the coarse-scale data generated by the GCM is accurate, we conclude that although more computationally demanding than the other two techniques, kriging seems to represent a good compromise between computational complexity and accuracy. Contrary to bicubic interpolation, kriging generates values within the range of
15   values generated by the GCM and generates more reliable variability indices than the bilinear interpolation.

Because the GCM generated reliable temperatures at coarse grain which were highly correlated with the CRU present-day temperatures, the three interpolation techniques produced similar linear splines and led to relatively similar values for this variable. The IPSL-CM5A-LR GCM is known to predict lower temperatures than observed at high latitudes in winter
20   (Dufresne et al., 2013). This bias was indeed observed when comparing the interpolated temperature with the CRU present-day data. As a result, the spline for temperature had a shallow slope at low temperature (Fig. 1). This correction was emphasised for the LGM data generated by the GCM in winter in the North of Europe (Fig. S11), which are outside of the range of present-day temperature, and therefore relied on a linear interpolation of the spline. No palynological or vertebrate data were available to evaluate the performance of the downscaling method in this region, and such a correction should be
25   treated with caution. For the purpose of studying the spatial distribution of modern human population, this overcorrection will have negligible effects, since this region was covered by an ice cap during the time of interest, and the range of values over the whole region in the present-day data encompasses the range of values for the region where humans were present during the LGM (Figs. S2-S7).

30   Our goal in this research has been to develop and test tools for the production of climate simulations at a suitable scale to investigate the mechanisms through which climate change and locally decision-making may have affected broader evolutionary patterning in the archaeological record. Our results demonstrate the potential of GAMs for the production of climate simulations at a fine scale of resolution, both spatially and temporally, at low computational cost. The resulting climate simulations can be used to test human decision-making at regional and local scales, particularly with regards to the

spatial distribution of prehistoric populations against a backdrop of inter and intra-annual climate variability (Burke et al. 2017; Burke et al. 2014). The impact of climate change on human decision-making processes at a local scale, specifically the selection of seasonal ranges within annual territories, will have had a cumulative effect leading to the larger-scale patterning currently discussed in the literature. Paleoclimatological models, such as the ones produced here, also allow climatologists to

5 investigate climate events that are not observable in the present – such as sudden climate change – but which may occur in the near future. Collaboration with archaeologists, who produce chronologically controlled datasets, allowed us to evaluate the simulation outputs at a fine scale of resolution.

Code and data availability. The code used for the downscaling and the input and output data are available at at

10 https://figshare.com/s/1b952e47ff274cc0687e (DOI: 10.6084/m9.figshare.5487145).

Author contributions. GLa, AB, MK, MV and GLe conceived the study. GLa and GLe implemented the R code for the downscaling. MK, MV and GR ran the IPSL-CM5A-LR simulations and implemented the code for the interpolations. CD implemented the code for the computation of the continentality. GL wrote the paper and all commented on it.

Competing interests. The authors declare that they have no conflict
of interest.

Acknowledgements. This research was supported by the *Fonds Québécois de Recherche Société et Culture - Programme de*

20 *soutien aux équipes* (demande no.179537).

References

Abe-Ouchi, A., Saito, F., Kageyama, M., Braconnot, P., Harrison, S. P., Lambeck, K., Otto-Bliesner, B. L., Peltier, W. R., Tarasov, L., Peterschmitt, J.-Y., and Takahashi, K. Ice-sheet configuration in the CMIP5/PMIP3 Last Glacial Maximum experiments, Geosci. Model Dev., 8, 3621-3637 2015.

25 Agnew, CT. Using the SPI to Identify Drought. Drought Network News (1994-2001), 5, 2000.

Akaike, H. A new look at the statistical model identification. IEEE T. Automat. Contr., 19(6), 716-723, 1974.

Banks, W.E., d'Errico, F., Peterson, A.T., Kageyama, M., Sima, A., and Sánchez-Goñi, M.F. Neanderthal extinction by competitive exclusion. PloS ONE, 3, e3972, 2008a.

Banks, W.E., d'Errico, F., Peterson, A.T., Vanhaeren, M., Kageyama, M., Sepulchre, P., Ramstein, G., Jost, A., and Lunt, D. Human ecological niches and ranges during the LGM in Europe derived from an application of eco-cultural niche modeling. J. Archaeol. Sci., 35, 481-491, 2008b.

Benito, BM., Svenning, J.-C., Kellberg-Nielsen, T., Riede, F., Gil-Romera, G., Mailund, T., Kjaergaard, P.C., and Sandel, B.S. The ecological niche and distribution of Neanderthals during the Last Interglacial. J. Biogeogr., 44(1):51-61, 2017.

Braconnot, P., Harrison, S. P., Otto-Bliesner, B., Abe-Ouchi, A., Jungclaus, J., and Peterschmitt, J.-Y. The Paleoclimate Modeling Intercomparison Project contribution to CMIP5, CLIVAR Exchanges No. 56, Vol. 16, No.2, May 2011, pp 15-19, 2011

Braconnot, P., Harrison, S. P., Kageyama, M., Bartlein, P. J., Masson-Delmotte, V., Abe-Ouchi, A., Otto-Bliesner, B., and Zhao, Y. Evaluation of climate models using palaeoclimatic data, Nat. Clim. Change, 2(6), 417-424, 2012.

Bradtmöller, M., Pastoors, A., Weninger, B., and Weniger, G. C. The repeated replacement model–rapid climate change and population dynamics in Late Pleistocene Europe. Quatern. Int., 247, 38-49, 2012.

Burke, A., Levavasseur, G., James, P.M.A., Guiducci, D., Izquierdo, M., Bourgeon, L., Ramstein, G., and Vrac, M. Exploring the impact of climate variability during the Last Glacial Maximum on the pattern of human occupation of Iberia. J. Hum. Evol., 73:35-46, 2014.

Burke, A., Kageyama, M., Latombe, G., Fasel, M., Vrac, M., Ramstein, G., and James, P.M.A. Risky business: The impact of climate and climate variability on human population dynamics in Western Europe during the Last Glacial Maximum. Quaternary Sci. Rev., 164:217-229, 2017.

Davies, W. and Gollop, P. The human presence in europe during the Last Glacial Period II. Climate tolerance and climate preferences of Mid-and Late Glacial hominids. Neanderthals and modern humans in the European landscape of the last glaciation, 131-146, 2003.

Delgado Huertas, A., Iacumin, P. and Longinelli, A. A stable isotope study of fossil mammal remains from the Paglicci cave, southern Italy, 13 to 33 ka BP: palaeoclimatological considerations. Chem. Geol., 141(3–4), p. 211-223, 1997.

Dufresne, J.-L., Foujols, M.A., Denvil, S., Caubel, A., Marti, O., Aumont, O., Balkanski, Y., Bekki, S., Bellenger, H., Benshila, R., Bony, S., Bopp, L., Braconnot, P., Brockmann, P., Cadule, P., Cheruy, F., Codron, F., Cozic, A., Cugnet, D., de Noblet, N., Duvel, J.-P., Ethé, C., Fairhead, L., Fichefet, T., Flavoni, S., Friedlingstein, P., Grandpeix, J.-Y., Guez, L., Guilyardi, E., Hauglustaine, D., Hourdin, F., Idelkadi, A., Ghattas, J., Joussaume, S., Kageyama, M., Krinner, G., Labetoulle, S., Lahellec, A., Lefebvre, M.-P., Lefevre, F., Levy, C., Li, Z. X., Lloyd, J., Lott, F., Madec, F. G., Mancip, M., Marchand, M., Masson, S., Meurdesoif, Y., Mignot, J., Musat, I., Parouty, S., Polcher, J., Rio, C., Schulz, M., Swingedouw, D., Szopa, S., Talandier, C., Terray, P., and Viovy, N.. Climate change projections using the IPSL-CM5 Earth System Model: from CMIP3 to CMIP5. Clim. Dynam., 40, 2123-2165, 2013.

Fasel M. STI: Calculation of the Standardized Temperature Index. R Package version 01 https://cran.r-project.org/web/packages/STI/, 2014.

Finlayson, C., Giles Pacheco, F., Rodriguez-Vidal, J., Fa, D.A., Maria Gutierrez Lopez, J., Santiago Perez, A., Finlayson, G., Allue, E., Baena Preysler, J., Caceres, I., Carrion, J.S., Fernandez Jalvo, Y., Gleed-Owen, C.P., Jimenez Espejo, F.J., Lopez, P., Antonio Lopez Saez, J., Antonio Riquelme Cantal, J., Sanchez Marco, A., Giles Guzman, F., Brown, K., Fuentes, N., Valarino, C.A., Villalpando, A., Stringer, C.B., Martinez Ruiz, F., and Sakamoto, T. Late survival of Neanderthals at the southernmost extreme of Europe. Nature 443, 850-853, 2006.

Finlayson, C., Fa, D.A., Jiménez Espejo, F., Carrión, J.S., Finlayson, G., Giles Pacheco, F., Rodríguez Vidal, J., Stringer, C., and Martínez Ruiz, F. Gorham's Cave, Gibraltar--The persistence of a Neanderthal population. Quatern. Int., 181, 64-71, 2008.

Flato, G., Marotzke, J., Abiodun, B., Braconnot, P., Chou, S.C., Collins, W., Cox, P., Driouech, F., Emori, S., Eyring, V., Forest, C., Gleckler, P., Guilyardi, E., Jakob, C., Kattsov, V., Reason, C., and Rummukainen, M. Evaluation of Climate Models. In: Climate Change 2013: The Physical Science Basis. Contribution of Working Group I to the Fifth Assessment Report of the Intergovernmental Panel on Climate Change [Stocker, T.F., D. Qin, G.-K. Plattner, M. Tignor, S.K. Allen, J. Boschung, A. Nauels, Y. Xia, V. Bex and P.M. Midgley (eds.)]. Cambridge University Press, Cambridge, United Kingdom and New York, NY, USA, 2013.

Gamble, C., Davies, W., Pettitt, P., and Richards, M. Climate change and evolving human diversity in Europe during the last glacial. Philos. T. Roy. Soc. B,359(1442), 243-254, 2004.

Gutowski Jr, W. J., Decker, S. G., Donavon, R. A., Pan, Z., Arritt, R. W., and Takle, E. S. Temporal–spatial scales of observed and simulated precipitation in central US climate. J. Climate, 16(22), 3841-3847, 2003.

Guttman, NB. Accepting the Standandardized Precipitation Index: a calculation algorithm. J. Amer. Water Resour. Assoc. 35(2), 311-322, 1999.

Hastie, T. J. and Tibshirani, R. J., 1990. Generalized Additive Models, Chapman and Hall.

Hernandez Fernandez, M. Análisis paleoecológico y paleoclimático de las sucesiones de mamíferos del Plio-Pleistoceno ibérico, Biologie. Universidad Complutense de Madrid, Madrid, p. 368, 2001a.

Hernandez Fernandez, M. Bioclimatic discriminant capacity of terrestrial mammal faunas. Global Ecol. Biogeogr., 10, 189-204, 2001b.

Hughes, J.K., Haywood, A., Mithen, S.J., Sellwood, B.W., and Valdes, P.J. Investigating early hominin dispersal patterns: developing a framework for climate data integration. J. Hum. Evol., 53(5):465-474,. 2007.

Huntley, B., Alfano, M. J., Allen, J. R., Pollard, D., Tzedakis, P. C., de Beaulieu, J. L., Grüger, E., and Watts, B.. European vegetation during marine oxygen isotope stage-3. Quaternary Res., 59(2), 195-212, 2003.

Jennings, R., Finlayson, C., Fa, D., and Finlayson, G. Southern Iberia as a refuge for the last Neanderthal populations. J. Biogeogr., 38(10), 1873-1885, 2011.

Jiménez-Espejo, F. J., Martínez-Ruiz, F., Finlayson, C., Paytan, A., Sakamoto, T., Ortega-Huertas, M., Finlayson, C., Ijima, K., Gallego-Torres, D., and Fa, D. Climate forcing and Neanderthal extinction in Southern Iberia: insights from a multiproxy marine record. Quaternary Sci. Rev., 26(7), 836-852, 2007.

Iacumin, P. and Longinelli, A. Relationship between δ18O values for skeletal apatite from reindeer and foxes and yearly mean δ18O values of environmental water. Earth Planet. Sc. Lett., 201(1), p. 213-219, 2002.

IPCC, 2013: Climate Change 2013: The Physical Science Basis. Contribution of Working Group I to the Fifth Assessment Report of the Intergovernmental Panel on Climate Change [Stocker, T.F., D. Qin, G.-K. Plattner, M. Tignor, S.K. Allen, J.

5   Boschung, A. Nauels, Y. Xia, V. Bex and P.M. Midgley (eds.)]. Cambridge University Press, Cambridge, United Kingdom and New York, NY, USA, 1535 pp, 2013.

Kageyama, M., Braconnot, P., Bopp, L., Caubel, A., Foujols, M.-A., Guilyardi, E., Khodri, M., Lloyd, J., Lombard, F., Mariotti, V., Marti, O., Roy, T., and Woillez, M.-N. Mid-Holocene and Last Glacial Maximum climate simulations with the IPSL model. Part I: comparing IPSL_CM5A to IPSL_CM4. Clim. Dynam., 40, 2447-2468, 2013a.

10   Kageyama, M., Braconnot, P., Bopp, L., Mariotti, V., Roy, T., Woillez, M.-N., Caubel, A., Foujols, M.-A., Guilyardi, E., Khodri, M., Lloyd, J., Lombard, F., and Marti, O. Mid-Holocene and Last Glacial Maximum climate simulations with the IPSL model. Part II: model-data comparisons. Clim. Dynam., 40, 2469-2495, 2013b.

Kaplan, J. O., Bigelow, N. H., Prentice, I. C., Harrison, S. P., Bartlein, P. J., Christensen, T. R., Cramer, W., Matveyeva, N. V., McGuire, A. D., Murray, D. F., Razzhivin, V. Y., Smith, B., Walker, D. A., Anderson, P. M., Andreev, A. A., Brubaker,

15   L. B., Edwards, M. E., and Lozhkin, A. V. Climate change and arctic ecosystems II: Modeling, paleodata-model comparisons, and future projections. J. Geophys. Res., 108(D19), 8171, 2003.

Levavasseur, G., Vrac, M., Roche, D. M., Paillard, D., Martin, A., and Vandenberghe, J. Present and LGM permafrost from climate simulations: contribution of statistical downscaling, Clim. Past,7, 1225–1246, 2011.

Liang, X.-Z., Pan, J., Zhu, J., Kunkel, K. E., Wang, J. X. L., and Dai, A. Regional climate model downscaling of the u.s.

20   summer climate and future change, J. Geophys. Res.: Atmospheres (1984–2012),111(D10) , 2006.

Longinelli, A., Iacumin, P., Davanzo, S., and Nikolaev, V. Modern reindeer and mice: revised phosphate–water isotope equations. Earth Planet. Sc. Lett., 214(3–4), p. 491-498, 2003.

López-García, J. M., Blain, H. A., Cuenca-Bescós, G., Ruiz-Zapata, M. B., Dorado-Valiño, M., Gil-García, M. J., Valdeolmillos, A., Ortega, A.I., Carretero, J.M., Arsuaga, J.L., Bermúdezde Castroe, J.M., and Carbonell, E.

25   Palaeoenvironmental and palaeoclimatic reconstruction of the latest Pleistocene of El Portalón site, Sierra de Atapuerca, northwestern Spain. Palaeogeogr. Palaeocl., 292(3), 453-464, 2010.

López-García, J. M., Blain, H.-A., Bennàsar, M., Euba, I., Bañuls, S., Bischoff, J., López-Ortega, E., Saladié, P., Uzquiano, P. and Vallverdú, J. A multiproxy reconstruction of the palaeoenvironment and palaeoclimate of the Late Pleistocene in northeastern Iberia: Cova dels Xaragalls, Vimbodí-Poblet, Paratge Natural de Poblet, Catalonia. Boreas, 41(2), 235-249,

30   2011a.

López-García, J. M., Cuenca-Bescós, G., Blain, H. A., Álvarez-Lao, D., Uzquiano, P., Adán, G., Arbizu, M. and Arsuaga, J. L. Palaeoenvironment and palaeoclimate of the Mousterian–Aurignacian transition in northern Iberia: The small-vertebrate assemblage from Cueva del Conde (Santo Adriano, Asturias). J. Hum. Evol., 61(1), 108-116, 2011b.

López-García, J. M., Cuenca-Bescós, G., Finlayson, C., Brown, K., and Pacheco, F. G. Palaeoenvironmental and palaeoclimatic proxies of the Gorham's cave small mammal sequence, Gibraltar, southern Iberia. Quatern. Int., 243(1), 137-142, 2011c.

McKee, T.D., Doesken, N.J., and Kleist, J. The relationship of drought frequency and duration to time scales. . Proceedings of the 8th Conference of Applied Climatology. Anaheim, California: American Meterological Society. p 179-184, 1993.

Mix, A. C., Bard, E., and Schneider, R. Environmental processes of the ice age: land, oceans, glaciers (EPILOG), Quaternary Sci. Rev., 20, 627-657, 2001.

Müller, U.C., Pross, J., Tzedakis, P.C., Gamble, C., Kotthoff, U., Schmiedl, G., Wulf, S., and Christanis, K. The role of climate in the spread of modern humans into Europe. Quaternary Sci. Rev., 30, 273-279, 2011.

New, M., Lister, D., Hulme, M., and Makin, I. A high-resolution data set of surface climate over global land areas, Clim. Res., 21(1), 1-25, 2002.

Palombo, M. R., Filippi, M. L., Iacumin, P., Longinelli, A., Barbieri, M., and Maras, A. Coupling tooth microwear and stable isotope analyses for palaeodiet reconstruction: the case study of Late Middle Pleistocene Elephas (Palaeoloxodon) antiquus teeth from Central Italy (Rome area). Quatern. Int., 126–128(0), p. 153-170, 2005.

Sanchez Goñi, M. F., and Harrison, S. P. Millennial-scale climate variability and vegetation changes during the Last Glacial: Concepts and terminology.Quaternary Sci. Rev., 29(21), 2823-2827, 2010.

Schmidt, I., Bradtmöller, M., Kehl, M., Pastoors, A., Tafelmaier, Y., Weninger, B., and Weniger, G. C. Rapid climate change and variability of settlement patterns in Iberia during the Late Pleistocene. Quatern. Int., 274, 179-204, 2012.

Sepulchre, P., Ramstein, G., Kageyama, M., Vanhaeren, M., Krinner, G., Sánchez-Goñi, M. F., and d'Errico, F.. H4 abrupt event and late Neanderthal presence in Iberia. Earth Planet. Sc. Lett., 258(1), 283-292, 2007.

Serangeli, J. and Bolus, M. Out of Europe - The dispersal of a successful European hominin form. Quartar 55, 83-98, 2008.

Shea, J.J. Transitions or turnovers? Climatically-forced extinctions of Homo sapiens and Neanderthals in the east Mediterranean Levant. Quaternary Sci. Rev., 27, 2253-2270, 2008.

Tallavaara, M., Luoto, M., Korhonen, N., Järvinen, H., and Seppä, H. Human population dynamics in Europe over the Last Glacial Maximum. P. Natl. Acad. Sci. USA, 112(27):8232-8237, 2015.

Taylor, K.E., R.J. Stouffer, R.J. and Meehl, G.A. An Overview of CMIP5 and the experiment design." Bull. Amer. Meteor. Soc, 93, 485-498, 2012.

van Andel, T.H. and Davies, W. Neanderthals and Modern Humans in the European Landscape of the Last Glaciation: Archaeological results of the stage 3 project. McDonald Institute for Archaeological Research Monographs, Cambridge, 2003.

Vita-Finzi, C. and Higgs, E. Prehistoric Economy in the mount Carmel area of Palestine: Site catchment analysis. P. Prehist. Soc., 36, 1970.

Vaittinada Ayar, P., Vrac, M., Bastin, S., Carreau, J., Déqué, M., and Gallardo, C. Intercomparison of statistical and dynamical downscaling models under the EURO- and MED-CORDEX initiative framework: Present climate evaluations. Clim Dyn, 46: 1301, 2016.

Vicente-Serrano, S.M., Beguería, S., and López-Moreno, J.I. A multiscalar drought index sensitive to global warming: the standardized precipitation evapotranspiration index. J. Climate, 23(7):1696-1718, 2010.

Vrac, M., Marbaix, P., Paillard, D., and Naveau, P. Non-linear statistical downscaling of present and LGM precipitation and temperatures over Europe. Clim. Past, 3(4), 669-682, 2007.

Walter, H. and Box, E. Global classification of natural terrestrial ecosystems. Vegetatio, 32(2), 75-81, 1976.

Wolff, E. W., Chappellaz, J., Blunier, T., Rasmussen, S. O., and Svensson, A. Millennial-scale variability during the last glacial: The ice core record.Quaternary Sci. Rev., 29(21), 2828-2838, 2010.

Wood, A. W., Leung, L. R., SRidhar, V., and Lettenmaier, D. P. Hydrologic implications of dynamical and statistical approaches to downscaling climate model outputs, Clim. Change, 62, 189–216, 2004.

Wood, S. N. Modelling and Smoothing Parameter Estimation with Multiple Quadratic Penalties, J. R. Stat. Soc. B, 62(2), 413-428, 2000.

Wood, S. N. Stable and efficient multiple smoothing parameter estimation for generalized additive models, J. Am. Stat. Assoc., 99(467), 2004.

Wood S. Generalized additive models: an introduction with R. Chapman and Hall/CRC, Boca Raton, FL, 2006.

Wu, H., Guiot, J., Brewer, S., and Guo, Z. Climatic changes in Eurasia and Africa at the last glacial maximum and mid-Holocene: reconstruction from pollen data using inverse vegetation modelling, Clim. Dynam., 29(2-3), 211-229, 2007.

Yokoyama, Y., Lambeck, K., De Deckker, P., Johnston, P., and Fifield, L. K. Timing of the Last Glacial Maximum from observed sea-level minima. Nature, 406(6797), 713-716, 2000.

Table 1. Model selection among all possible combinations of variables for the temperature and the precipitations. Only the five models with the lowest AIC are presented. AIC scores, differences in AIC compared to the lowest scoring model (Δ_{AIC}), and AIC weights (w_{AIC}) are reported.

Candidate model	AIC	Δ_{AIC}	w_{AIC}
Bilinear interpolation			
Temperature			
T+elv+Aco	869468.4	0	1
T+elv	878862.9	9394.52	0
T+Aco	951357.5	81889.14	0
T	955986.9	86518.50	0
elev+Aco	1605682.9	736214.55	0
Precipitations			
T+P+elev+Aco+RH+SLP	275068.7	0	1
T+P+elev+Aco+SLP	281222.3	6153.56	0
T+P+elev+Aco+RH	283266.4	8197.70	0
T+P+elev+RH+SLP	288574.6	13505.85	0
T+P+elev+Aco	288864.1	13795.35	0
Bicubic interpolation			
Temperature			
T+elv+Aco	896517.0	0	1
T+elv	904724.6	8207.52	0
T+Aco	952109.7	55592.63	0
T	955079.5	58562.43	0
elev+Aco	1605402.4	708885.36	0
Precipitations			
T+P+elev+Aco+RH+SLP	274137.9	0	1
T+P+elev+Aco+SLP	278178.8	4040.881	0
T+P+elev+Aco+RH	283162.3	9024.412	0
T+P+elev+Aco	286857.5	12719.589	0
T+P+elev+RH+SLP	286926.3	12788.379	0
Kriging			
Temperature			
T+elv+Aco	878970.1	0	1
T+elv	888326.4	9356.24	0
T+Aco	952033.1	73062.92	0
T	956903.8	77933.70	0
elev+Aco	1607626.2	728656.08	0
Precipitations			
T+P+elev+Aco+RH+SLP	269767.4	0	1
T+P+elev+Aco+SLP	276171.0	6403.59	0
T+P+elev+Aco+RH	277692.0	7924.60	0
T+P+elev+Aco	283099.2	13331.79	0
T+P+Aco+RH+SLP	286495.6	16728.23	0
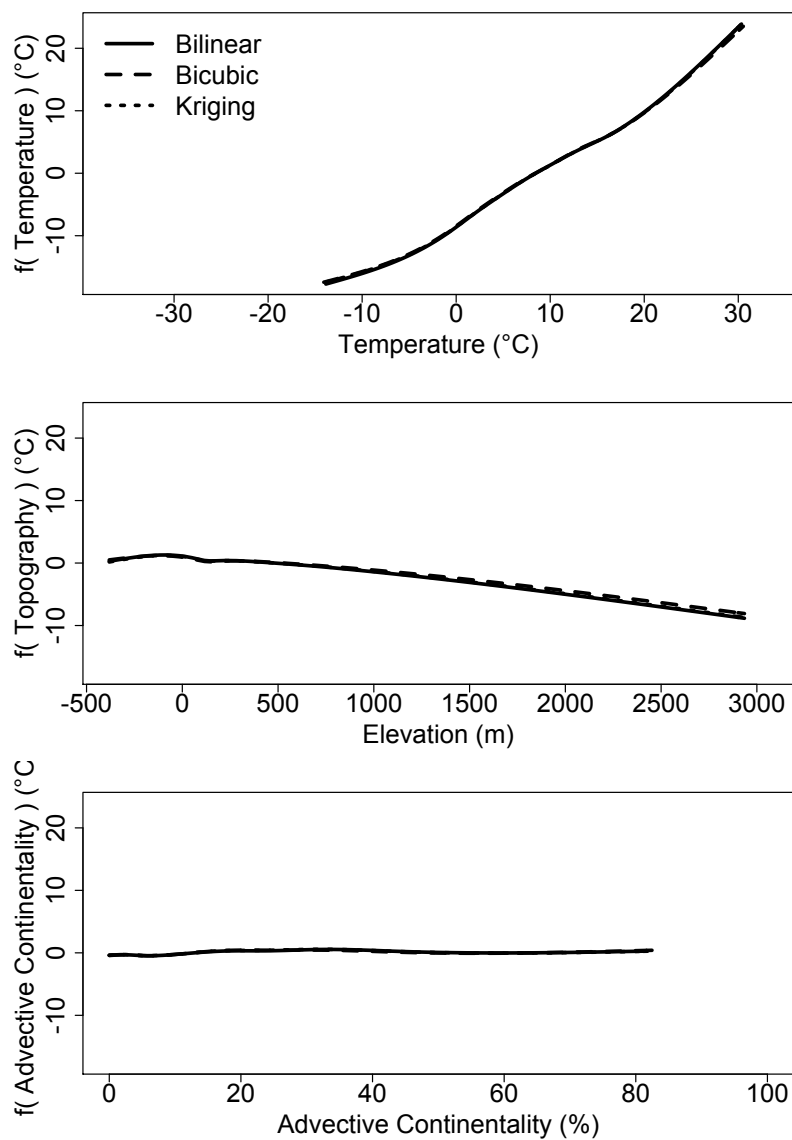
Figure 1. Splines of the GAM for temperature. The splines are scaled to the same range to allow for visual estimation of their
5   **relative importance.**

Figure 2. Histograms of the predictor variables for the present-time (1960-1990; solid lines) and for the LGM (dashed lines) over Western Europe, using the bilinear (red), bicubic (green) and kriging (blue) interpolations.
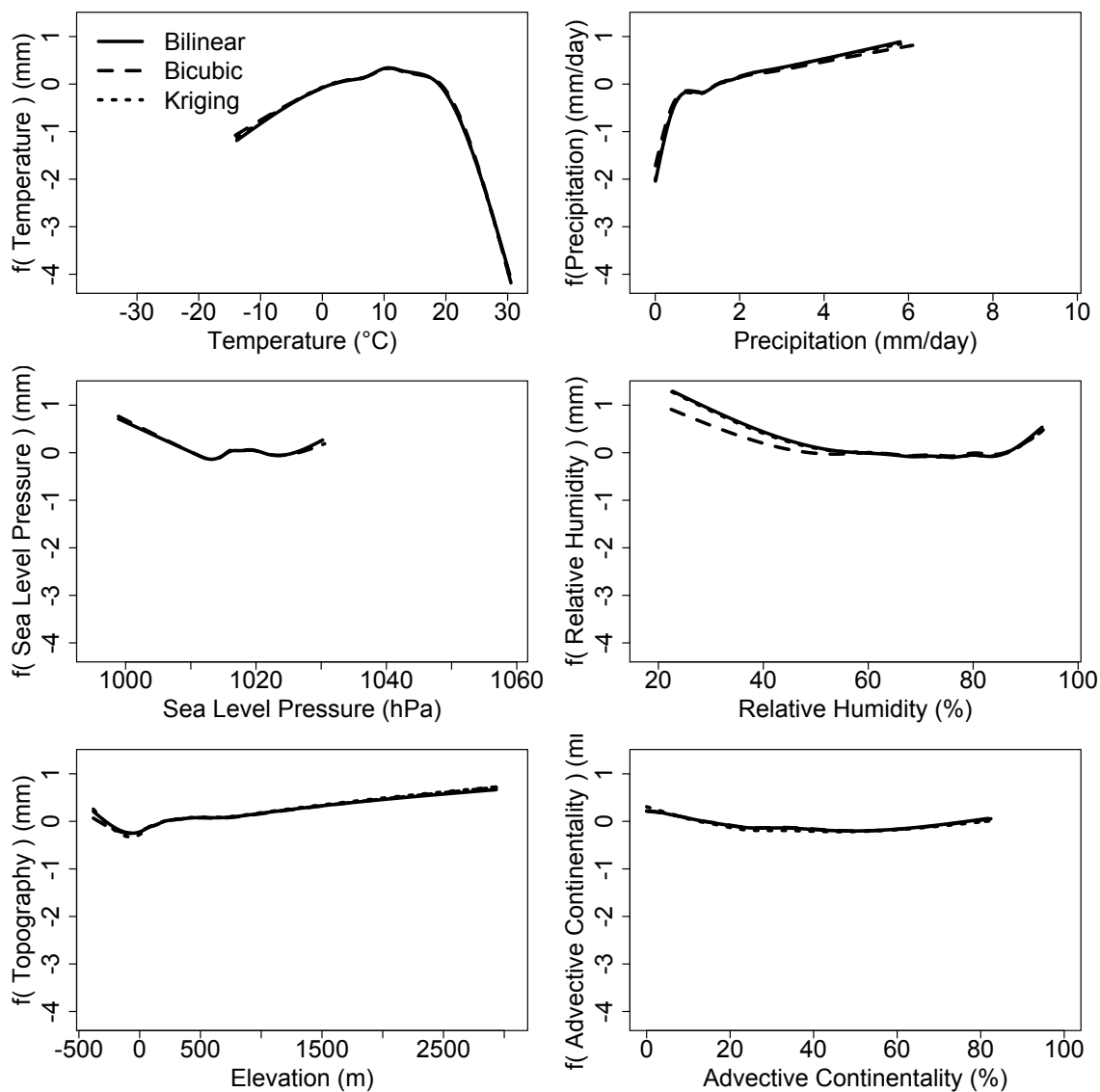
Figure 3. Splines of the GAM for precipitations. The splines are scaled to the same range to allow for visual estimation of their relative importance.
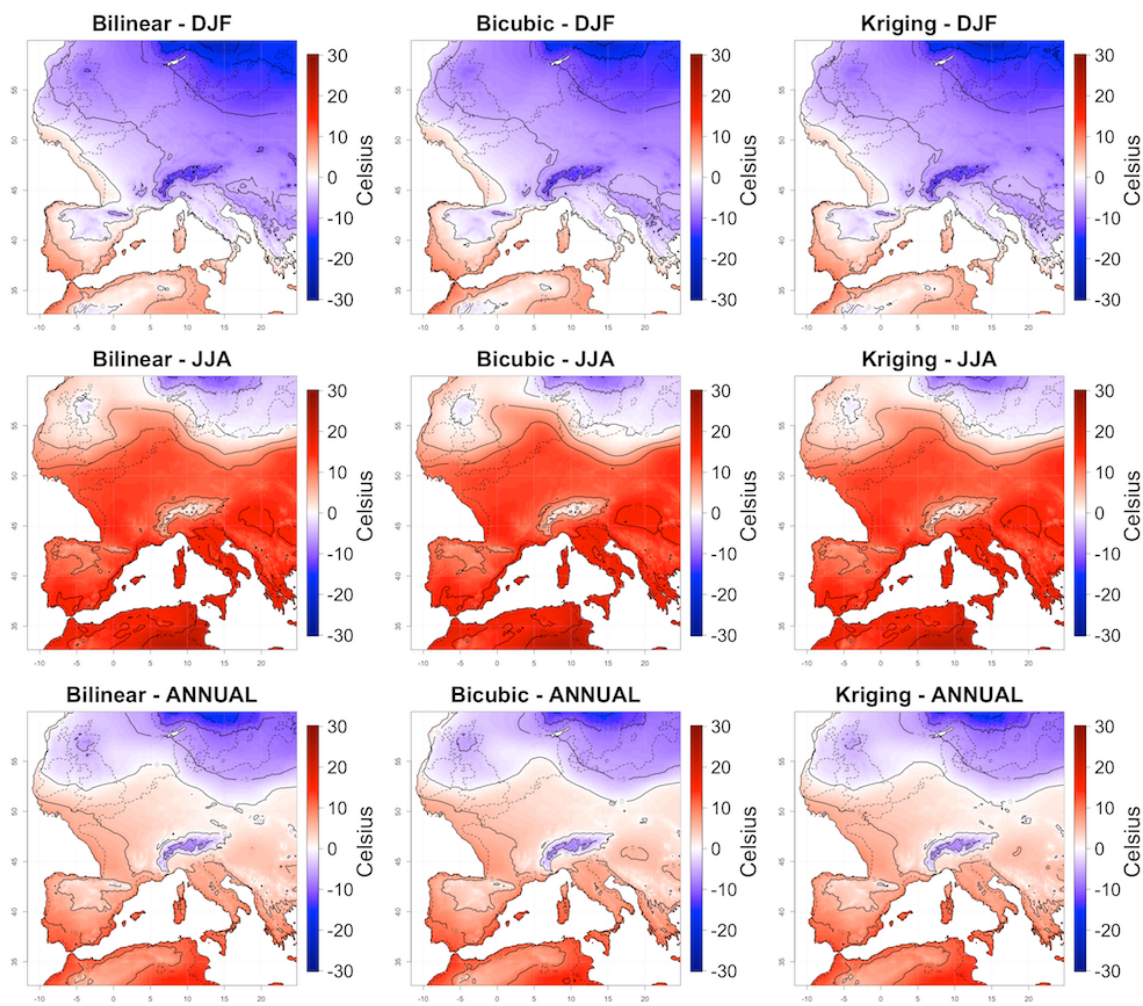
Figure 4. Maps of mean distributions of monthly mean downscaled temperatures over Western Europe during the LGM for winter (December, January, February), summer (June, July, August), and the whole year, computed over 50 years for the three interpolation techniques.
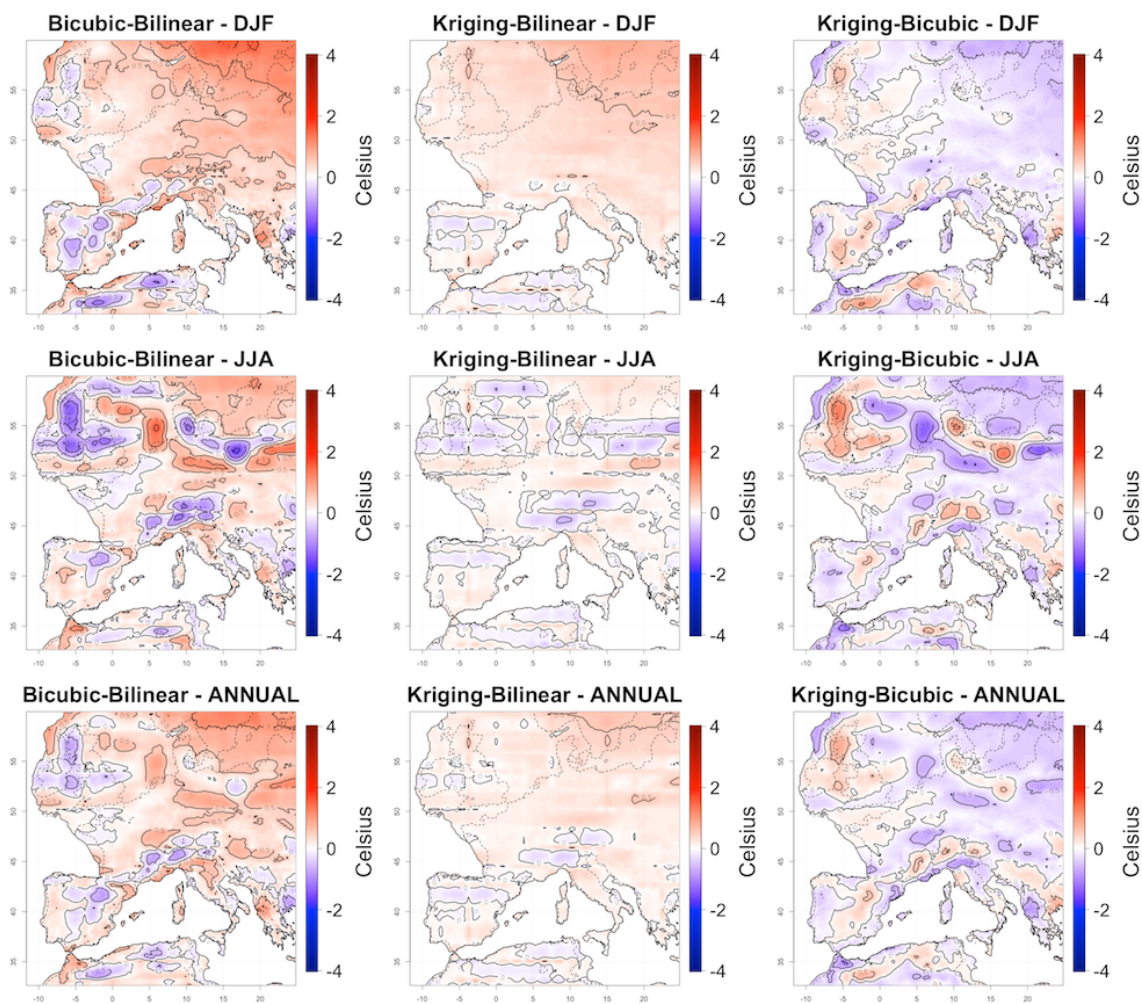
Figure 5. Maps of difference in mean distributions of monthly mean downscaled temperatures over Western Europe during the LGM for winter (December, January, February), summer (June, July, August), and the whole year, computed over 50 years, between the three interpolation techniques.
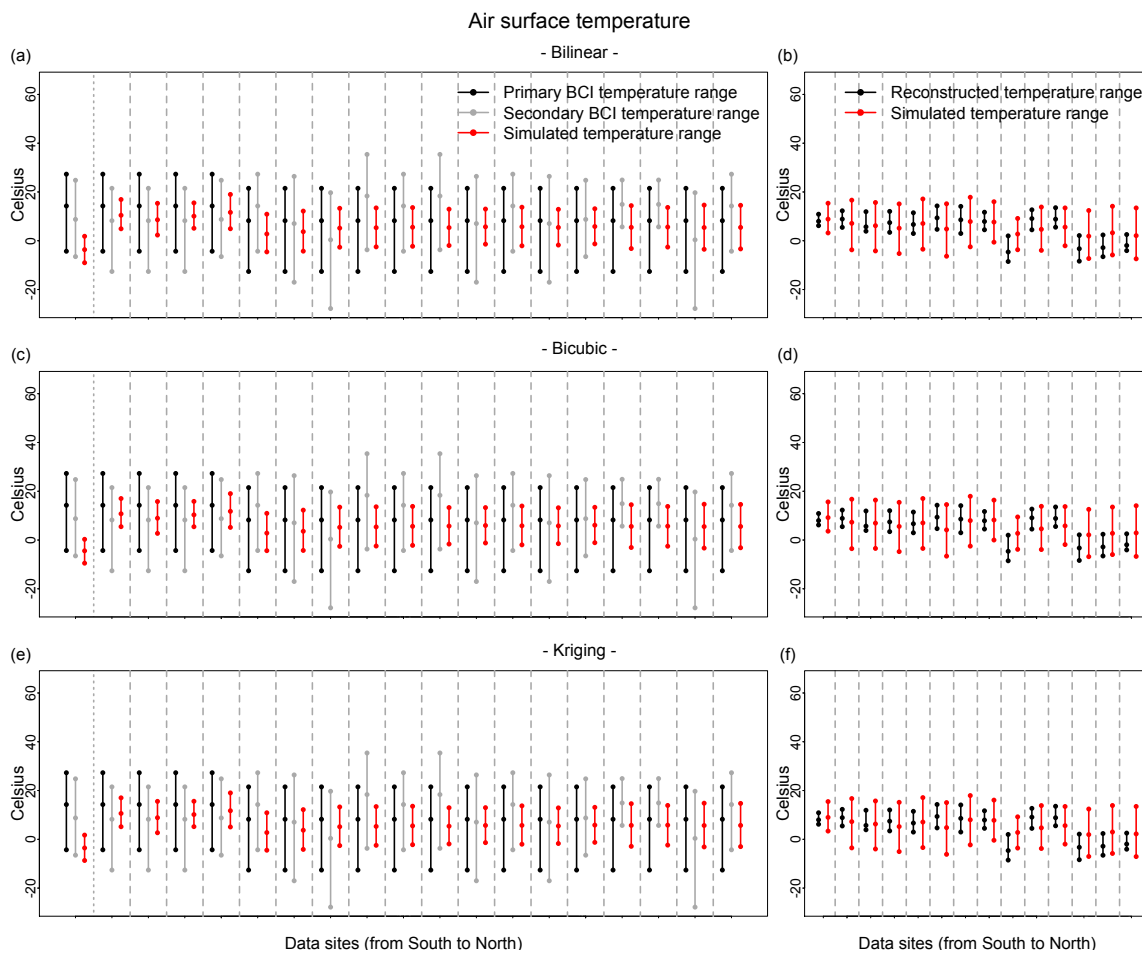
Figure 6. Boxplot of reconstructed vs. downscaled, simulated temperatures for the LGM based on the BCI indices (a, c, e), and from Wu et al. (2007)'s reconstructions (b, d, f).
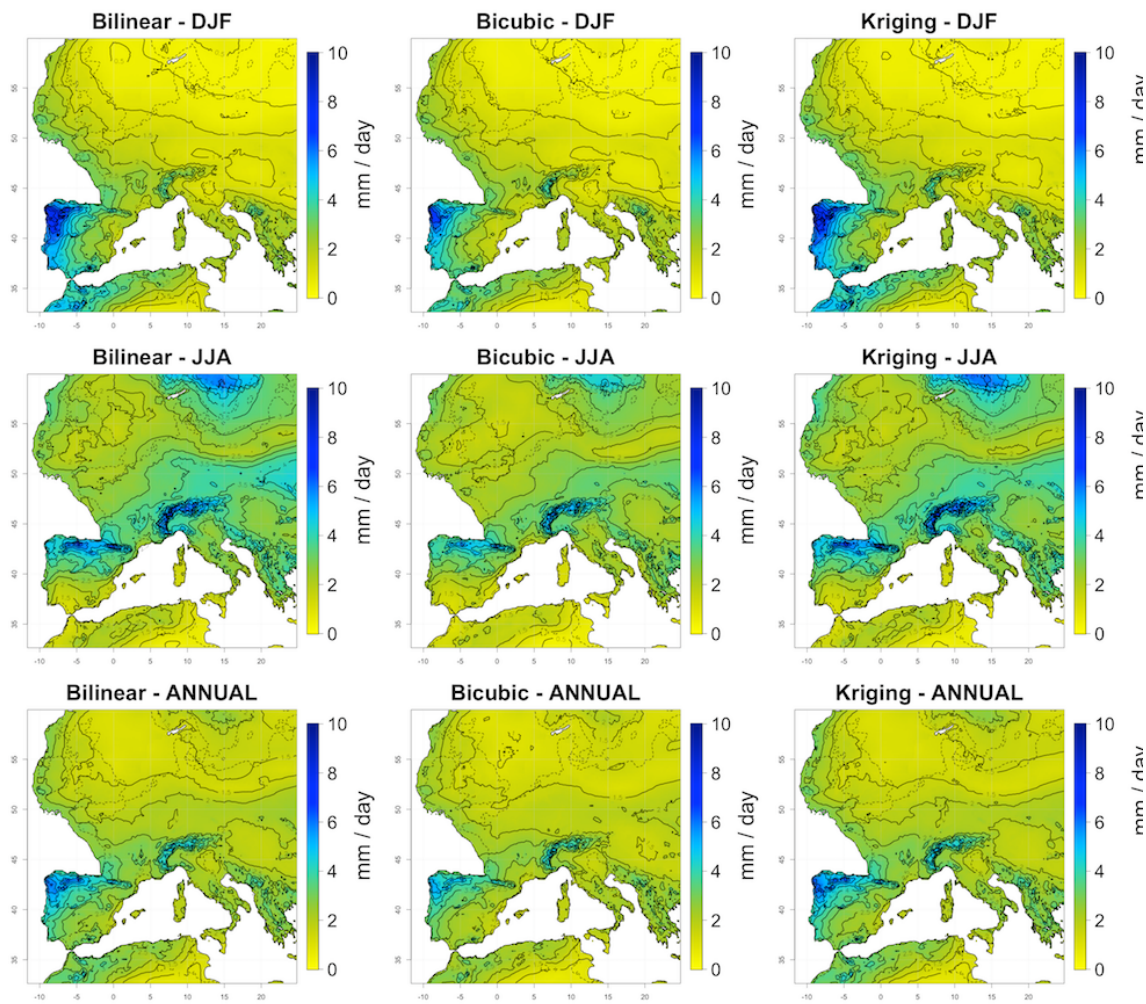
Figure 7. Maps of mean distributions of downscaled daily precipitations over Western Europe during the LGM for winter (December, January, February), summer (June, July, August), and the whole year, computed over 50 years for the three interpolation techniques.
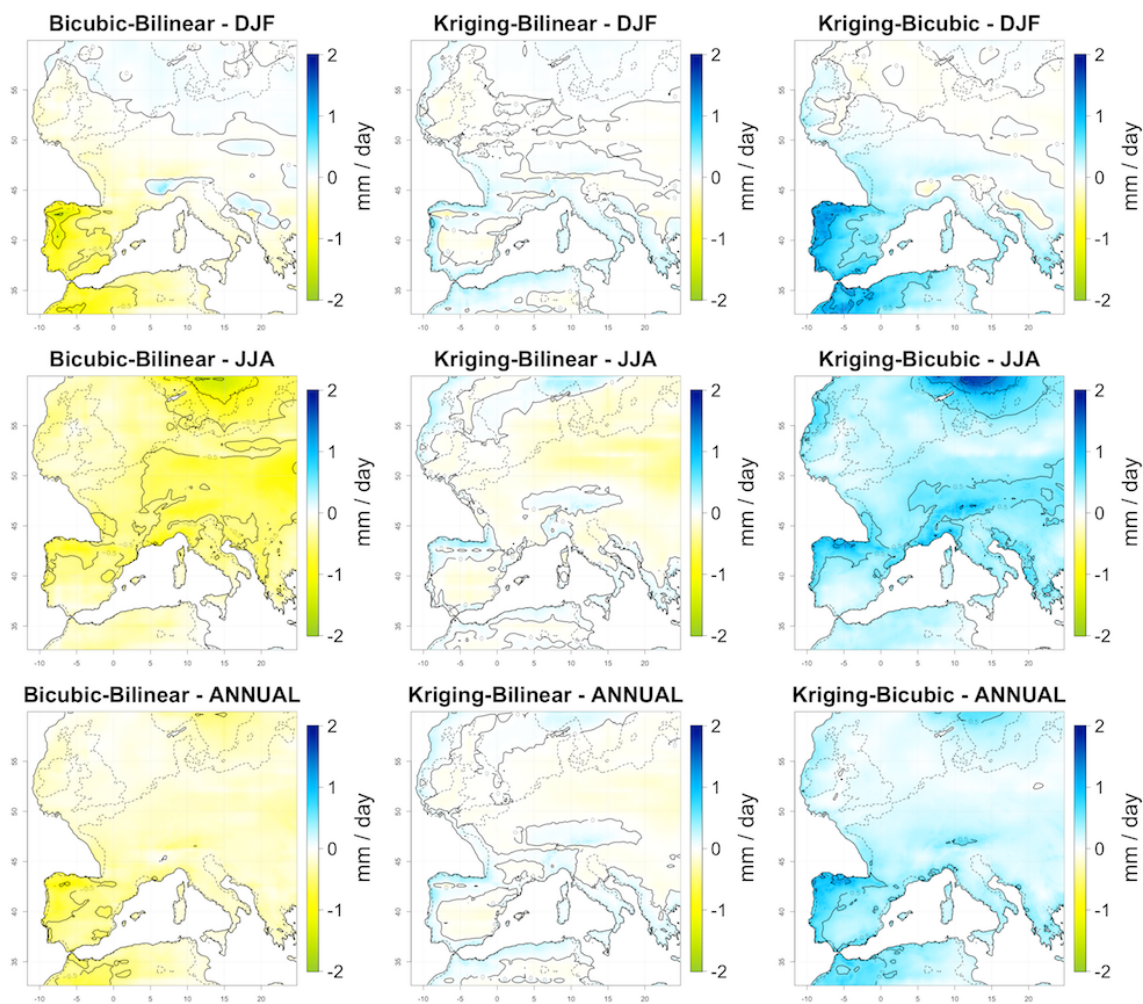
Figure 8. Maps of difference in mean distributions of downscaled daily precipitations over Western Europe during the LGM for winter (December, January, February), summer (June, July, August), and the whole year, computed over 50 years, between the three interpolation techniques.
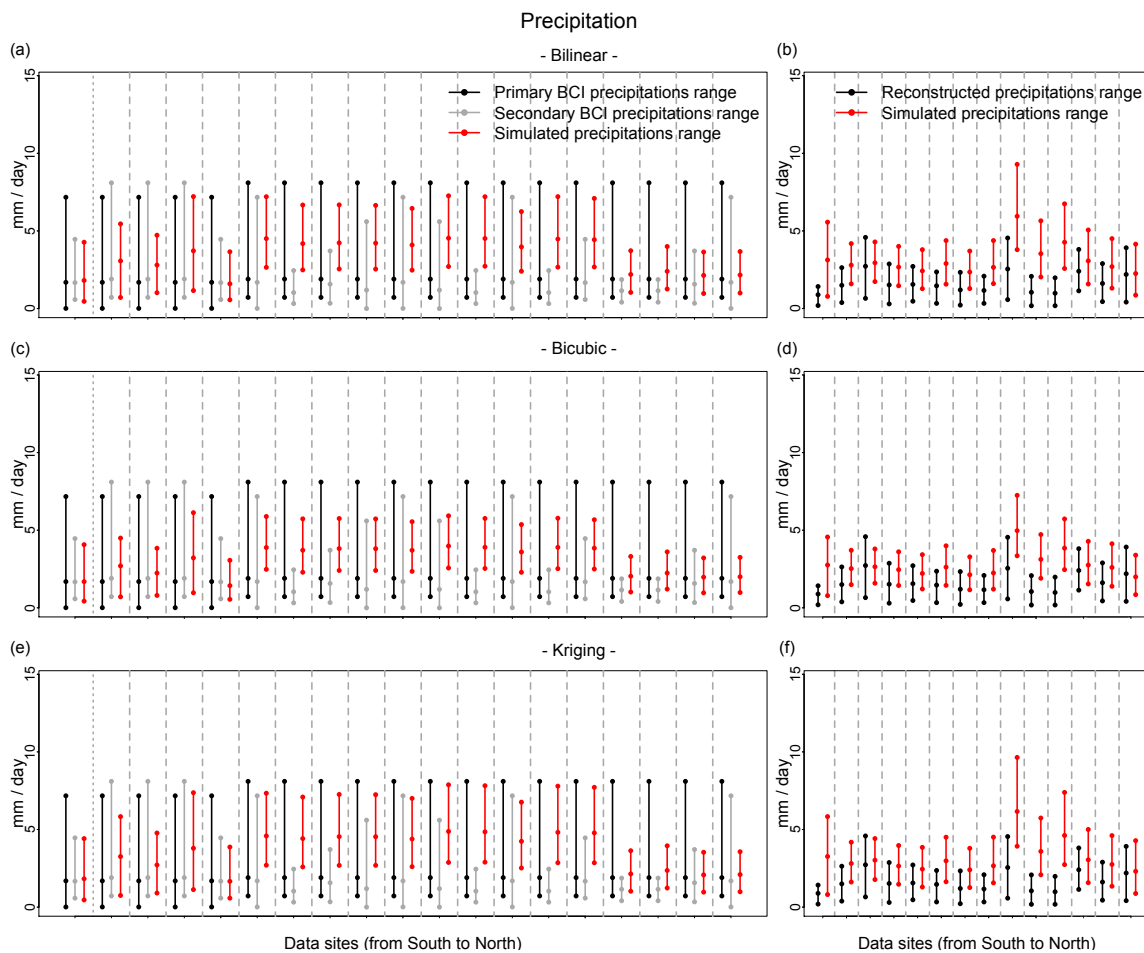
Figure 9. Boxplot of reconstructed vs. downscaled, simulated precipitations for the LGM based on the BCI indices (a, c, e), and from Wu et al. (2007)'s reconstructions (b, d, f).
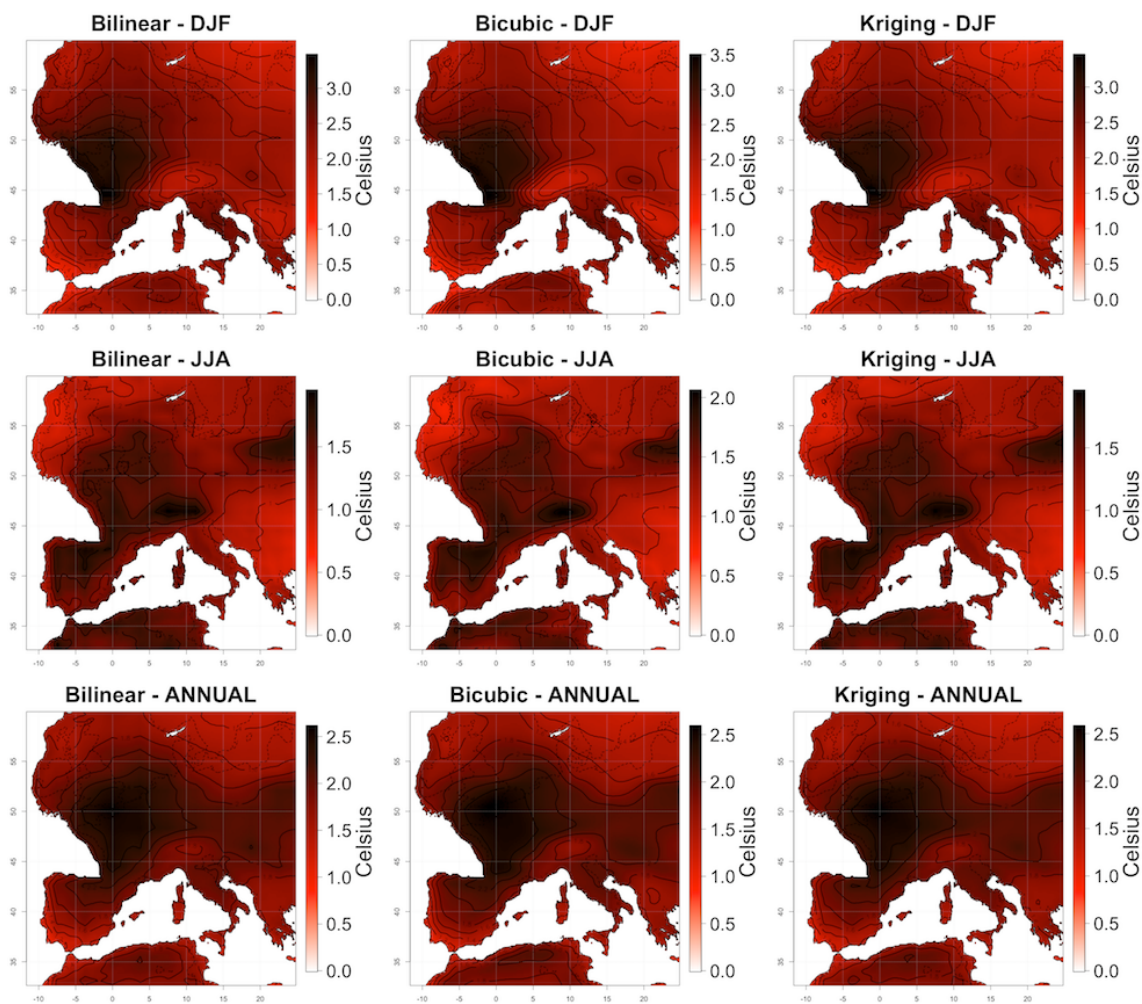
Figure 10. Maps of temporal variations (standard deviation of each month across 50 years) of downscaled monthly mean temperatures over Western Europe during the LGM averaged over winter (December, January, February), summer (June, July, August), and the whole year for the three interpolation techniques. Color scales differ between maps for better distinguishing the spatial artifacts.
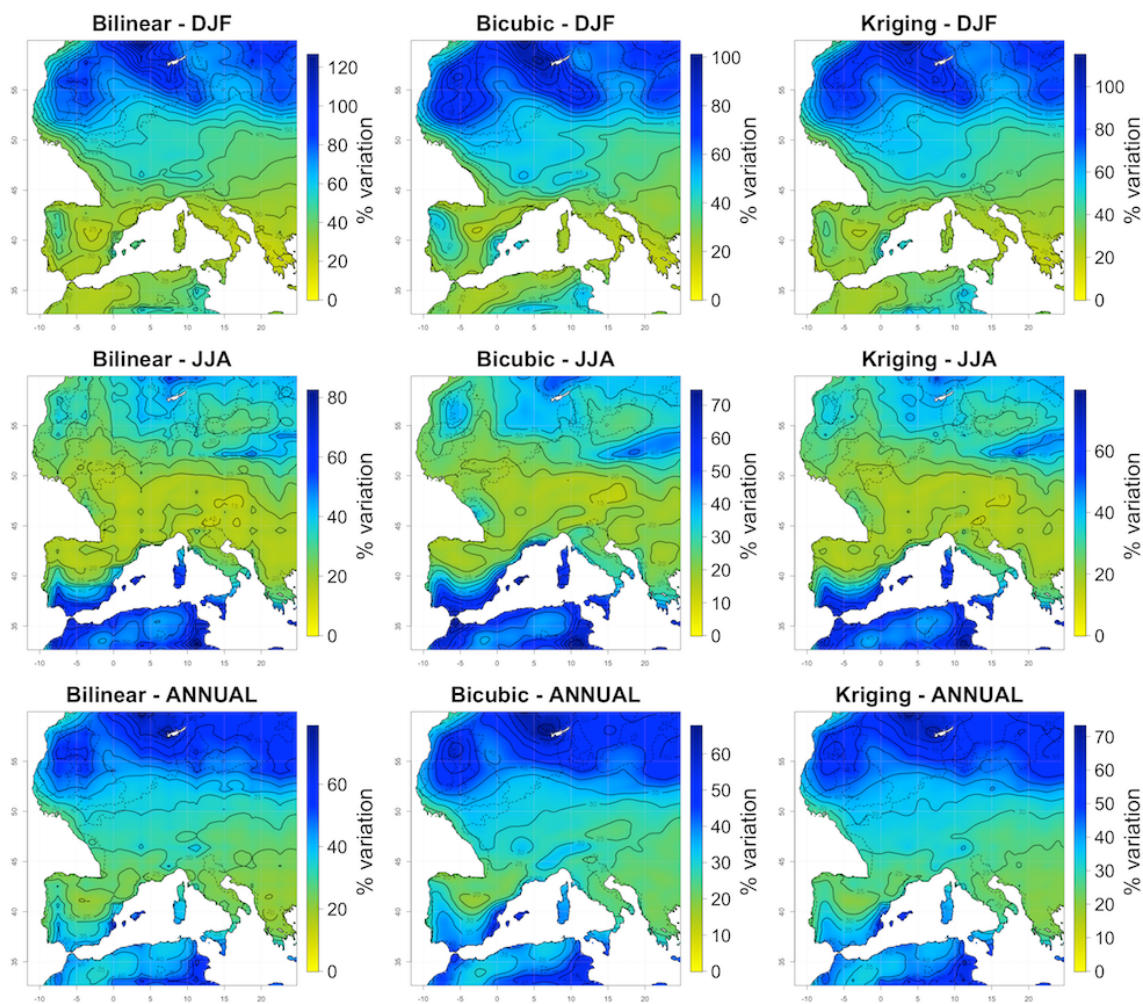
Figure 11. Maps of temporal variations (coefficient of variation of each month across 50 years) of downscaled daily precipitations over Western Europe during the LGM averaged over winter (December, January, February), summer (June, July, August), and the whole year, computed over 50 years for the three interpolation techniques. Color scales differ between maps for better distinguishing the spatial artifacts.